Passive non-linear microrheology for determining extensional viscosity

Kai-Wen Hsiao,[1] Jelena Dinic,[2] Yi Ren,[1] Vivek Sharma,[2] and Charles M. Schroeder[1,a)]
[1]*Department of Chemical and Biomolecular Engineering, University of Illinois at Urbana-Champaign, 600 S Mathews Avenue, Urbana, Illinois 61801, USA*
[2]*Department of Chemical Engineering, University of Illinois at Chicago, 810 S Clinton St., Chicago, Illinois 60607, USA*

(Received 30 June 2017; accepted 9 August 2017; published online 6 October 2017)

Extensional viscosity is a key property of complex fluids that greatly influences the non-equilibrium behavior and processing of polymer solutions, melts, and colloidal suspensions. In this work, we use microfluidics to determine steady extensional viscosity for polymer solutions by directly observing particle migration in planar extensional flow. Tracer particles are suspended in semi-dilute solutions of DNA and polyethylene oxide, and a Stokes trap is used to confine single particles in extensional flows of polymer solutions in a cross-slot device. Particles are observed to migrate in the direction transverse to flow due to normal stresses, and particle migration is tracked and quantified using a piezo-nanopositioning stage during the microfluidic flow experiment. Particle migration trajectories are then analyzed using a second-order fluid model that accurately predicts that migration arises due to normal stress differences. Using this analytical framework, extensional viscosities can be determined from particle migration experiments, and the results are in reasonable agreement with bulk rheological measurements of extensional viscosity based on a dripping-onto-substrate method. Overall, this work demonstrates that non-equilibrium properties of complex fluids can be determined by passive yet non-linear microrheology. *Published by AIP Publishing.* https://doi.org/10.1063/1.4993736

I. INTRODUCTION

Bulk measurements of stress and viscosity are essential to understand the non-equilibrium behavior of complex fluids. Macroscopic stress-strain relations in structured materials such as polymer solutions or colloidal suspensions are known to arise due to molecular-scale behavior and dynamic microstructural effects. To this end, flow-induced particle migration is a phenomenon that illustrates the connection between bulk stresses and microscopic interactions in fluids. Particle migration has long been observed in various complex fluids including suspensions,[1–3] polymer solutions,[4–6] and multi-component materials such as blood flows that exhibit margination,[7,8] known as the Fahraeus-Lindqvist effect.[9]

Flow-induced migration can arise due to several different phenomena, including hydrodynamic interactions with boundaries,[10] inertial effects,[11] or viscoelastic effects due to stress gradients in flowing fluids.[12,13] Particle migration in viscoelastic materials was first experimentally observed in shear flow by Karnis and Mason,[4] where it was found that spherical particles suspended in polyisobutylene (PIB) solutions migrated towards the direction of minimum shear rate, which corresponds to the channel center-line in a pressure-driven Poiseuille flow. Leal and co-workers used a second-order fluid model to quantitatively understand this phenomenon and attributed migration to normal stress due to lateral variations in shear rate.[12,13] In addition to polymer solutions, particle migration has also been studied in colloidal suspensions.[14–17] Morris and co-workers developed an experimental apparatus to measure the osmotic pressure change resulting from shear-induced particle migration in particulate suspensions,[18] where it was found that changes in pressure varied linearly with shear rate and were related to normal stress. Particle migration in polymer solutions has also been studied using microfluidics,[19] including methods to determine relaxation times in polymer solutions in uniform channels.[20] Recently, a new microfluidic method to precisely focus particles was demonstrated using a combination of inertial and elastic focusing effects.[21] Despite recent progress on studying particle migration phenomena in flow, however, the vast majority of prior work on flow-induced migration has nearly exclusively focused on shear flow or uniform flow in channels.

Unlike shear flow, purely extensional flows consist only of extensional/compressional character with no elements of fluid rotation, which is known to generate strong stress responses in polymeric materials. The flow properties of polymer solutions in extensional flow have been studied using rheo-optical techniques such as flow birefringence,[22–28] filament stretching rheometry,[29–31] capillary breakup extensional rheometry (CABER),[32–37] drop break-up in microchannels,[38–41] jetting-based extensional rheometry,[42,43] and dripping-onto-substrate (DoS) extensional rheometry.[44–46] Ober *et al.* developed a microfluidic-based "indexing" method to estimate extensional viscosity by measuring mechanical pressure drop across a hyperbolic contraction geometry using on-chip fabricated pressure sensors;[47] however, given the complex mixture of shear and extensional flow components in this geometry, it is challenging to determine extensional viscosity using the approach.[47,48] Pressure drop measurements across cross-slot

a)Electronic mail: cms@illinois.edu

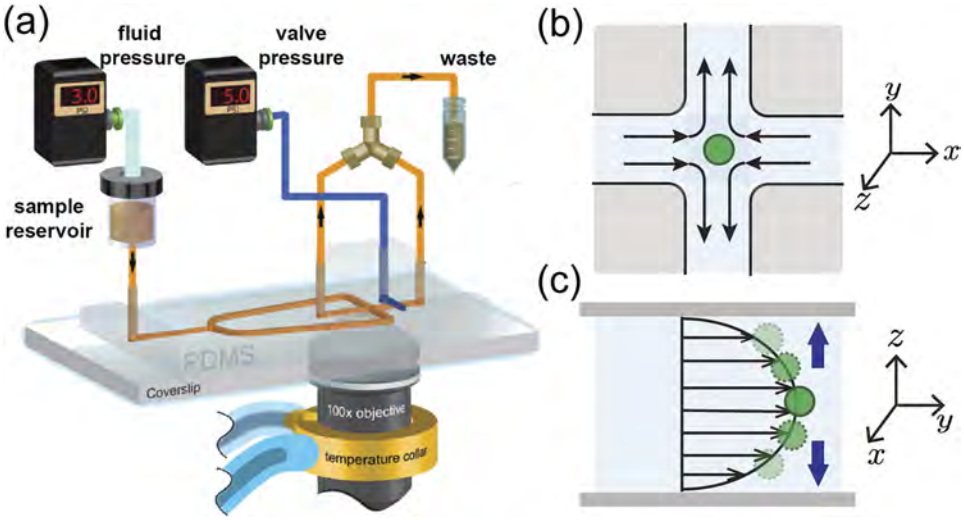

FIG. 1. Schematic of the experimental setup for studying particle migration in planar extensional flow. (a) Schematic of a PDMS cross-slot microfluidic device with automated pressure-driven flow control. (b) Top-down view of a cross-slot device showing planar extensional flow in the x-y plane. (c) Side view of a microfluidic channel showing particle migration in the direction transverse to flow (z-direction) towards the top and bottom confining surfaces. The strain rate $\dot{\epsilon}(z)$ is a function of position in the z-direction.

flow geometries are generally more amenable to determining extensional viscosity by separating the effects of shear flow and extensional flow,[43,49] though recent work has highlighted difficulties in separating the contributions of shear and extension-generated normal stresses in several microfluidic geometries.[48] Taken together, there are ongoing challenges in using microfluidics to measure extensional flow properties for complex fluids.

In this work, we directly observe particle migration in semi-dilute polymer solutions in planar extensional flow (Fig. 1). Microfluidic experiments are performed in the regime of negligible inertia (Reynolds number $Re \ll 1$), such that particle migration occurs due to finite normal stresses in the flowing polymer solution. Particle migration trajectories are analyzed in the context of a second-order fluid model,[12,13] which enables determination of steady extensional viscosity under moderate flow rates. In our work, planar extensional flow is generated in a cross-slot microfluidic device using pressure-driven flow, resulting in a two-dimensional velocity profile in the x-y plane with a strain rate $\dot{\epsilon}(z)$ that varies in the transverse direction (z-direction) (Fig. 1). Single tracer particles suspended in polymer solutions are trapped in two-dimensions near the stagnation point using an active feedback control method known as a Stokes trap.[50,51] In semi-dilute polymer solutions, particles are observed to migrate towards the channel walls in the direction transverse to flow (z-direction), which is consistent with prior experimental[4] and theoretical studies[12,13] of particle migration in shear flow showing that particles tend to migrate in the direction of decreasing shear rate due to normal stress effects. Using this approach, we present the direct observation of particle migration in viscoelastic polymer solutions in extensional flow, coupled with detailed analysis of these experimental data in order to determine extensional viscosity using microfluidics.

II. EXPERIMENTAL APPROACH

A. Polymer solutions and bulk rheological characterization

We prepared three different semi-dilute polymer solutions based on a biopolymer (DNA) and a synthetic polymer (polyethylene oxide, PEO). Semi-dilute DNA solutions (λ-DNA, Invitrogen, 48.5 kbp, $M = 3.2 \times 10^7$ g/mol) are prepared in viscous aqueous solutions (60% w/w sucrose, 30 mM Tris-HCl, pH 8.0, 0.1 mM EDTA, and 5 mM NaCl) at two different concentrations corresponding to 1 c^* and 2.5 c^*, where c^* is the polymer overlap concentration ($c^* = 40$ μg/ml for λ-DNA[52]), as previously described.[53] The solvent viscosity η_s of the 1 c^* and 2.5 c^* DNA solutions was 55 cP and 60 cP, respectively (Table I). Semi-dilute solutions of PEO (Sigma-Aldrich, average $M_w = 1.0 \times 10^6$ g/mol) are prepared in aqueous solutions at a concentration of 10 c^* (1.7% w/w). In all cases, polymer solutions are well-mixed and homogeneous, and experiments are conducted using a circulating water bath thermally coupled to microfluidic devices to maintain a constant temperature (22 °C).

Prior to microfluidic experiments, the bulk rheological properties of DNA and PEO solutions were determined, including zero-shear viscosity η_0 (Table I) and steady shear viscosity (Fig. S1 of the supplementary material). Zero-shear viscosity measurements and linear viscoelastic measurements were performed using a Discovery Hybrid Rheometer 3 (40 mm parallel plate geometry). Flow sweep zero-shear viscosity measurements on 1 c^* λ-DNA, 2.5 c^* λ-DNA, and 10 c^* PEO solution were conducted, and zero-shear viscosity η_0 is measured and reported as shown in Fig. S1. Linear viscoelastic measurements (frequency sweep measurements) on 10 c^* PEO solutions are shown in Fig. S2 of the supplementary material. For semi-dilute DNA solutions, longest relaxation times τ were determined using single molecule analysis by direct observation of single polymer relaxation,[53] together with the scaling relation $\tau/\tau_o \sim (c/c^*)^{0.48}$, where τ_o is the

TABLE I. Polymer solution properties measured using bulk rheology, including solvent viscosity η_s, zero-shear viscosity η_0, and longest relaxation time τ.

Sample	c	η_s (Pa s)	η_0 (Pa s)	τ (s)
1 c^* DNA	44 μg/ml	0.055	0.12	5.5
2.5 c^* DNA	100 μg/ml	0.060	0.31	6.5
10 c^* PEO	1.7 wt. %	0.001	0.37	0.01

longest polymer relaxation time in dilute solution. For semi-dilute PEO solutions, the longest relaxation time is obtained by linear viscoelastic measurements and DoS rheometry.

B. Stokes trap: Automated hydrodynamic trapping

Two-layer polydimethylsiloxane (PDMS) microfluidic devices are fabricated using standard techniques in soft lithography, such that a fluidic layer is situated below a control layer that contains a pressure-controlled valve.[53] The fluidic layer is designed to contain a cross-slot flow geometry that generates a planar extensional flow (Fig. 1). In this flow field, the velocity v in the x-y plane is given by $[v_x, v_y, v_z] = [-\dot{\epsilon}(z)(x - x_o), \dot{\epsilon}(z)(y - y_o), 0]$, where (x_o, y_o) is the location of the stagnation point and $\dot{\epsilon}(z)$ is the strain rate. Fluidic microchannels have a width of 300 μm and a depth of 100 μm in the cross-slot region. Single particles are trapped in flow near the stagnation point using a feedback controlled technique known as a Stokes trap.[51] The details of the implementation of the trapping method have been presented in prior work.[50,53] In brief, single particles are trapped in a 2D extensional flow using the following procedure: (1) images of fluorescent particles in flow are captured using a charge-coupled device (CCD) camera, and particle positions are detected using a custom LabView program for image analysis, (2) a target particle (e.g., fluorescent particle detected closest to the stagnation point) is selected for trapping, and (3) the target particle is confined in the flow plane (x-y plane) by actuating the on-chip membrane valve situated above one outlet channel (Fig. 1), which enables fine-scale modulation of the location of the stagnation point via slight changes to the fluidic resistance in one outlet flow line with respect to the other in the 4-channel cross-slot geometry. In this work, the action of the membrane valve results in negligible changes in the strain rate $\dot{\epsilon}$.[53]

C. Particle tracking velocimetry (PTV) for characterizing flow kinematics

Before studying particle migration in extensional flow, particle tracking velocimetry (PTV) was used to determine flow field kinematics and strain rates $\dot{\epsilon}$ in polymer solutions (Fig. 2), which allows for determination of a dimensionless flow strength known as the Weissenberg number $Wi = \dot{\epsilon}\tau$. A trace amount of fluorescent microbeads (0.84 μm diameter, Spherotech, 0.01% v/v) was added to polymer solutions to enable particle tracking. Microfluidic devices are mounted on an inverted fluorescence microscope (Olympus IX71), which allows for real-time imaging of fluorescent beads using a high numerical aperture (1.45 NA, 100×) oil-immersion objective lens and a solid-state CW laser (Coherent, 488 nm). Polymer solutions are introduced into microfluidic devices using a pressure regulator (Proportion Air), and images of bead positions are acquired as functions of applied pressure and z-position using a CCD camera (AVT Stingray). A custom particle tracking and analysis program is used to determine strain rates $\dot{\epsilon}$ for all polymer solutions, which allows for determination of a dimensionless flow strength known as the Weissenberg number $Wi = \dot{\epsilon}\tau$. Unless otherwise stated, Wi values are defined based on the strain rate $\dot{\epsilon}$ at the channel mid-plane. In all cases, the flow field was observed to be stable with no evidence of elastic instabilities.[54] Moreover, the strain rate profile in the z-direction was found to be parabolic (Fig. 2), which suggests small departures from Newtonian flow behavior at low to moderate Wi.

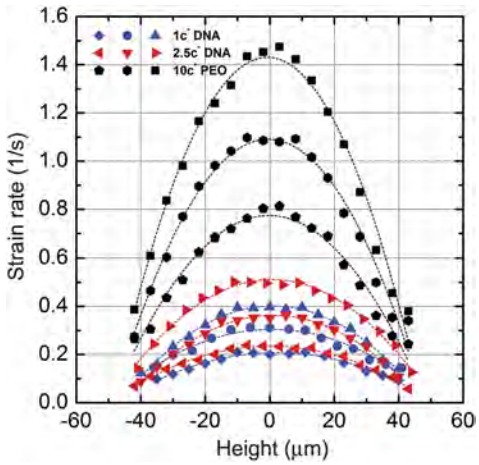

FIG. 2. Strain rates in planar extensional flow obtained from particle tracking velocimetry (PTV) as a function of z-position. Experimental data are shown as solid symbols and parabolic fits are shown as dashed lines, with 1 c^* DNA solution at Wi = 1.1 (◆), 1.6 (●), 2.1 (▲), and 2.5c^* DNA solution at Wi = 1.4 (◀), 2.1 (▼), and 3.3 (▶), and 10 c^* PEO solution at Wi = 0.008 (⬟), 0.011 (⬢), and 0.015 (■).

D. Piezo-nanopositioning stage for particle migration

Following flow field characterization, we studied particle migration in extensional flows of semi-dilute polymer solutions. The experiment begins by introducing a polymer solution containing a trace amount of fluorescent particles (0.84 μm diameter) into a microfluidic device via pressure-driven flow. Single particles are trapped in flow using a Stokes trap, and particle migration in the transverse direction (z-direction) is tracked using a piezo-nanopositioning stage (Physik Instrumente) and a custom control scheme (Fig. 3). In brief, the particle tracking algorithm is used to control the piezo stage to maintain a trapped fluorescent particle in focus during migration in the z-direction. The piezo stage is first initialized near the center plane of the microdevice (within 1–2 μm), and the area of the trapped particle is measured via an image analysis routine in LabView. As the particle migrates in the z-direction and begins to drift out of the focal plane, the piezo stage adjusts its position (up or down) such that the detected area of the particle is minimized. In this way, the z-position of the particle is recorded during the experiment. For reference, we show a few characteristic single particle migration trajectories from our experiments, together with the measured particle area as a function of time (Fig. S3 of the supplementary material). In these experiments, the particle position is sampled at 10 Hz.

E. Dripping-onto-substrate (DoS) rheometry

Dripping-onto-substrate (DoS) experiments are used to determine the bulk extensional viscosity of polymer solutions, as previously reported (Fig. 4).[44,45] The necks formed between a nozzle and a substrate for the PEO and DNA

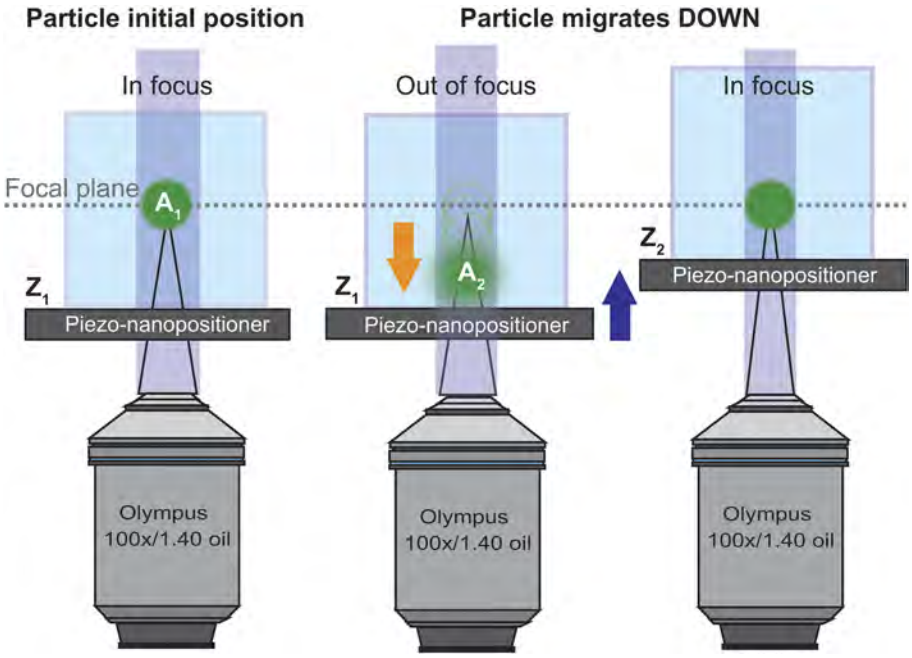

FIG. 3. Schematic of experimental approach for monitoring particle migration in the transverse direction (z-direction) in flow. In all cases, the piezo positioning stage moves in the direction that minimizes the particle area. Here we illustrate the case when a particle migrates downward. (Left) At the start of the experiment, the trapped particle is near the center of the channel. (Center) The particle migrates in the $-z$-direction. (Right) The piezo stage moves up to maintain the particle in focus.

solutions are cylindrical slender filaments, characteristic of high viscosity or high elasticity fluids,[34,44,45,55] which are distinct from conical necks associated with inviscid fluids or power law fluids.[45,56] The values of stress $\sigma/R(t)$ and extension rates $\dot{\epsilon} = -2\,(d\,\ln\,R(t)/dt)$ are calculated from radius $R(t)$ evolution data, where representative plots are shown in Figs. S4–S6 of the supplementary material. Transient and steady extensional viscosities are obtained from the radius evolution data using the following equation:

$$\eta_E = \frac{\sigma/R(t)}{\dot{\epsilon}(t)}. \tag{1}$$

Extensional viscosity obtained using capillary-thinning based methods such as CaBER,[32,34] DoS rheometry,[44,45] and jetting-based rheometry[43] are typically plotted as a function of the Hencky strain or the total accumulated strain $\epsilon = 2\,\ln\,(R_o/R(t))$ in the liquid filament that continuously increases as the neck radius $R(t)$ thins over time. Radius evolution data in the final regime before pinch-off for the aqueous PEO solutions and DNA solutions show a linear decrease with time, which can be captured by visco-capillary (VC) scaling relation,[57–59]

$$\frac{R(t)}{R_o} = 0.0709\frac{\sigma}{\eta_E R_o}(t_p - t), \tag{2}$$

where R_o is the initial radius, t_p is the pinch-off time, and η_E is the extensional viscosity. The presence of the terminal regime allows for the measurement of terminal steady extensional viscosity that is independent of both extension rate and strain. The

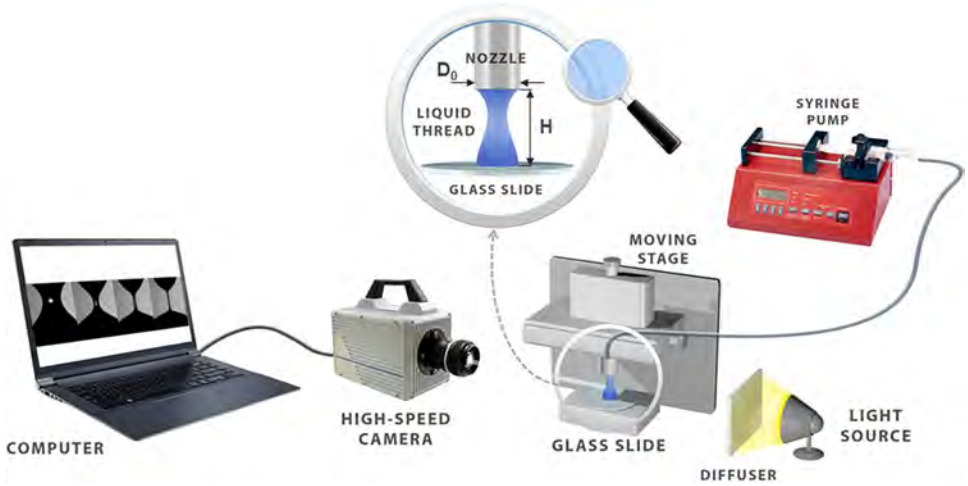

FIG. 4. Schematic of Dripping-onto-Substrate (DoS) rheometry setup.[44–46] A syringe pump is used for pumping a discrete volume of fluid at a relatively low flow rate Q through a nozzle (outer diameter $D_o = 2R_o = 1.270$ mm and inner diameter $D_i = 0.838$ mm) placed at a height H (aspect ratio $H/D_i \approx 3$) above a glass substrate. An unstable stretched liquid bridge is formed, bounded by the nozzle and a sessile drop on the substrate. The necked region undergoes capillary-driven self-thinning and pinch-off that are visualized using a Photron Fastcam SA3 high-speed camera equipped with a Nikkor 3.1× zoom lens (18–55 mm) and an additional super macrolens. The illumination system consists of a light source and a diffuser. The neck shape and diameter are determined using custom code written in MATLAB from images captured at a rate of 5000–8000 fps.

terminal steady extensional viscosity value is arguably a true material response[60,61] that depends on both molecular weight and polymer concentration, but not on the extension rate or the accumulated strain.[61–63]

III. ANALYTICAL THEORY

A. Particle migration in an extensional flow of a second-order fluid

In order to quantitatively understand microfluidic experiments, we sought to develop an analytical model to describe the migration of particles in viscoelastic solutions in an extensional flow. The migration of rigid spheres in a general quadratic flow of a second-order fluid was previously considered by Leal and Chan using analytical arguments.[13] Their results show that particle migration occurs due to normal stresses whenever a lateral variation in shear rate occurs in the undisturbed flow.[12] The second-order fluid model is useful for slowly varying flows of viscoelastic fluids ($Wi \lesssim 1$), and it provides a rational basis for separating the effects induced by normal stresses from those due to viscosity-dependent flow rates, mainly because the shear dependence of viscosity only enters at third-order in the expansion.[64] For these reasons, we adapted the theory of Leal and Chan[13] to the case of particle migration in planar extensional flow with a z-dependent strain rate.

An analytical expression for the dimensionless migration velocity $(\tilde{U}_s)_i$ of a rigid sphere in a general quadratic flow of a second-order fluid is given by[13]

$$(\tilde{U}_s)_i = \frac{5}{18}(5+13\epsilon_1)e_{nm}\psi_{mni} + \frac{1}{27}(1+11\epsilon_1)\epsilon_{imn}e_{ml}\theta_{ln} + \frac{1}{3}(1+3\epsilon_1)e_{im}\gamma_{mnn}, \tag{3}$$

where ϵ_{ijk} is the Levi-Civita tensor and e_{ij}, ψ_{ijk}, and θ_{ij} are the symmetric and irreducible tensorial components of the velocity coefficient tensors β_{ij} and γ_{ijk} for a general quadratic flow. Here, an irreducible tensor is defined to contract to zero along any two indices, such that $\beta_{ii} = \gamma_{iji} = \gamma_{iij} = 0$.

To obtain the particle migration velocity $(\tilde{U}_s)_i$, the individual terms in Eq. (3) need to be determined. To proceed, we introduce an expression for a dimensionless general quadratic velocity in a fixed frame,

$$\tilde{V}'_i = \alpha'_i + \beta'_{ij}\tilde{x}'_j + \gamma'_{ijk}\tilde{x}'_k\tilde{x}'_j, \tag{4}$$

where α'_i, β'_{ij}, and γ'_{ijk} are the constant velocity coefficient tensors and $\tilde{x}'_i$ is the dimensionless position vector relative the fixed frame (Fig. 5). For this derivation, it is preferred to adopt a coordinate system with the origin at the center of the particle, such that the coordinate system translates but does not rotate with the flow.[13] The dimensionless position vector in the translating coordinate frame is $\tilde{x}_i$. In this way, $\tilde{x}'_i = \tilde{x}_i + (\tilde{x}_0(t))_i$, where $(\tilde{U}_s)_i = (\tilde{x}_0(t))_i$ is the position vector for the center of rotation of the particle measured in the fixed frame, as shown in Fig. 5. Substituting this relation into Eq. (4), we obtain

$$\begin{aligned}\tilde{V}'_i = {} & [\alpha'_i + \beta'_{ij}(\tilde{x}_0(t))_j + \gamma'_{ijk}(\tilde{x}_0(t))_k(\tilde{x}_0(t))_j] \\ & + [\beta'_{ij} + 2\gamma'_{ijk}(\tilde{x}_0(t))_k]\tilde{x}_j + \gamma'_{ijk}\tilde{x}_k\tilde{x}_j,\end{aligned} \tag{5}$$

where we have used the symmetry condition $\gamma'_{ijk} = \gamma'_{ikj}$. We can now define a new set of velocity coefficient tensors in the translating frame α_i, β_{ij}, and γ_{ijk},

$$\begin{aligned}\alpha_i &= \alpha'_i + \beta'_{ij}(\tilde{x}_0(t))_j + \gamma'_{ijk}(\tilde{x}_0(t))_k(\tilde{x}_0(t))_j, \\ \beta_{ij} &= \beta'_{ij} + 2\gamma'_{ijk}(\tilde{x}_0(t))_k, \\ \gamma_{ijk} &= \gamma'_{ijk},\end{aligned} \tag{6}$$

where α_i and β_{ij} are time-dependent due to the translating coordinate frame, but γ_{ijk} is constant in time. We now arrive at an expression for the velocity in the fixed frame,

$$\tilde{V}'_i = \alpha_i + \beta_{ij}\tilde{x}_j + \gamma_{ijk}\tilde{x}_k\tilde{x}_j, \tag{7}$$

or, alternatively, an expression for the velocity in the translating frame,

$$\tilde{V}_i = \tilde{V}'_i - (\tilde{U}_s)_i = \alpha_i + \beta_{ij}\tilde{x}_j + \gamma_{ijk}\tilde{x}_k\tilde{x}_j - (\tilde{U}_s)_i. \tag{8}$$

Our goal is to solve for β_{ij} and γ_{ijk} in Eq. (8). The coefficients are related to the velocity field $\tilde{V}_i$ in the following relations:

$$\begin{aligned}\beta_{ij} &= \frac{\partial \tilde{V}_i}{\partial \tilde{x}_j}, \\ e_{ij} &= \tfrac{1}{2}(\beta_{ij} + \beta_{ji}), \\ \gamma_{ijk} &= \frac{\partial \tilde{V}_i}{\partial \tilde{x}_j \partial \tilde{x}_k}.\end{aligned} \tag{9}$$

Following Chan and Leal,[13] β_{ij} and γ_{ijk} can be decomposed into their respective irreducible components as follows:

$$\begin{aligned}\psi_{ijk} &= \frac{1}{6}(\gamma_{ijk} + \gamma_{ikj} + \gamma_{kij} + \gamma_{kji} + \gamma_{jik} + \gamma_{jki}) \\ &\quad - \frac{1}{15}(\gamma_{imm}\delta_{jk} + \gamma_{jmm}\delta_{ik} + \gamma_{kmm}\delta_{ij}), \\ \theta_{ij} &= \epsilon_{imn}\gamma_{nmj} + \epsilon_{jmn}\gamma_{nmi}, \\ \tau_i &= \gamma_{imm}.\end{aligned} \tag{10}$$

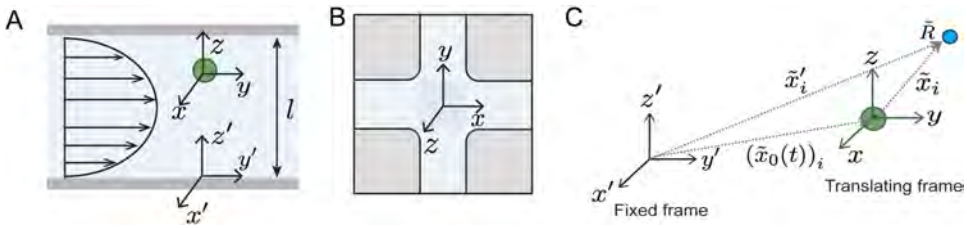

FIG. 5. Analytical model for studying particle migration in a planar extensional flow. (a) Schematic (side view) of flow profile in the microfluidic device, showing the fixed coordinate frame (x',y',z') and translating coordinate frame (x,y,z), the z-dependent strain rate $\dot{\epsilon}(z)$. Here, l is the dimensional channel height and $\tilde{z} = 0$ at the bottom surface. (b) Schematic (top-down view) of the microfluidic device, such that the fixed coordinate frame and translating coordinate frames are coincident in the x-y plane. (c) Particle position and velocity in a translating frame relative to the fixed laboratory frame.

Using this approach, we applied the analytical theory for particle migration in a second-order fluid to planar extensional flow. To begin, we define the locations of the fixed frame coordinate system given by (x',y',z') and the translating coordinate system given by (x,y,z), as shown in Fig. 5. The origin of fixed frame is located at the center of the cross-slot in the x-y plane and at the bottom of the microdevice, such that $z' = 0$ corresponds to the bottom wall. The particle is located an arbitrary distance δ away from the bottom wall. Clearly, the fixed frame and translating frame are coincident in the x-y plane, but not in the z-direction. The z-components of the coordinate systems are related by the relation: $z' = \delta + l\tilde{z}$, where $\tilde{z}$ is the dimensionless coordinate in the z-direction in the translating frame, rendered dimensionless with the microchannel height l. The expression for the dimensional undisturbed velocity field in the fixed frame is $[v_x', v_y', v_z'] = [-\dot{\epsilon}(z')(x' - x_o'), \dot{\epsilon}(z')(y' - y_o'), 0]$, where (x_o', y_o') is the location of the stagnation point and the z-dependent strain rate is $\dot{\epsilon}(z') = 4\dot{\epsilon}_{max}(z'/l)(1 - z'/l)$, shown schematically in Fig. 5 and validated by particle tracking experiments as shown in Fig. 2. The dimensionless strain rate can be expressed in the translating frame as $\tilde{\dot{\epsilon}}(\tilde{z}) = 4\tilde{\dot{\epsilon}}_{max}(\alpha + \tilde{z})(1 - \alpha - \tilde{z})$, where $\alpha = \delta/l$.

The problem reduces to determining the tensors e_{ij}, ψ_{ijk}, and θ_{ij} for the undisturbed velocity profile. To proceed, we solve for these terms using a dimensionless velocity profile $[\tilde{v}_x, \tilde{v}_y, \tilde{v}_z]$ and the dimensionless strain rate profile $\tilde{\dot{\epsilon}}(\tilde{z})$. The individual terms in the particle migration velocity given by Eqs. (3) and (10) are shown in Table II. Here, we define $i = 1$ to be the x-axis, $i = 2$ to be the y-axis, and $i = 3$ to be the z-axis. Combining the above relevant terms in Table II, including $e_{mn}\psi_{mni}$, $\epsilon_{imn}\epsilon_{ml}\theta_{ln}$, and $e_{im}\tau_m$, and Eq. (3), we obtain an expression for the particle migration velocity in the z-direction in a planar extensional flow,

$$\begin{aligned}(\tilde{U}_s)_z = {} & \tilde{\dot{\epsilon}}\left(\frac{d\tilde{\dot{\epsilon}}}{d\tilde{z}}\right)\left(\frac{10}{27}(5 + 13\epsilon_1) + \frac{4}{27}(1 + 11\epsilon_1)\right) \\ & + \left(\frac{d\tilde{\dot{\epsilon}}}{d\tilde{z}}\right)\left(\frac{d^2\tilde{\dot{\epsilon}}}{d\tilde{z}^2}\right)\left(\frac{2}{27}(5 + 13\epsilon_1) + \frac{1}{54}(1 + 11\epsilon_1) + \frac{1}{6}\right) \\ & \times \left((\tilde{x} - \tilde{x}_0)^2 + (\tilde{y} - \tilde{y}_0)^2\right). \end{aligned} \tag{11}$$

To simplify the analysis, we define the quantities $N_1(\epsilon_1) = \left(\frac{10}{27}(5 + 13\epsilon_1) + \frac{4}{27}(1 + 11\epsilon_1)\right)$ and $N_2(\epsilon_1) = \left(\frac{2}{27}(5 + 13\epsilon_1) + \frac{1}{54}(1 + 11\epsilon_1) + \frac{1}{6}\right)$. Moreover, $\Delta\tilde{x} = (\tilde{x} - \tilde{x}_0)$ and $\Delta\tilde{y} = (\tilde{y} - \tilde{y}_0)$ are assumed to be a trapped particle's instantaneous distance from the stagnation point $\tilde{x}_0$ and $\tilde{y}_0$ in the 2D plane. We assume that trapped particles exhibit symmetric and minor excursions from the stagnation point in the x-y plane, such that $\Delta\tilde{x} = \Delta\tilde{y} = 50\%$ of particle diameter a resulting in $2\Delta\tilde{x}^2 = 0.5$, which is consistent with prior experiments using the automated trap.[65] In this way, $(\tilde{x} - \tilde{x}_0)^2 + (\tilde{y} - \tilde{y}_0)^2 = 2\Delta\tilde{x}^2$, and Eq. (11) can be expressed as

$$\begin{aligned}(\tilde{U}_s)_z = {} & \tilde{\dot{\epsilon}}\left(\frac{d\tilde{\dot{\epsilon}}}{d\tilde{z}}\right)N_1(\epsilon_1) + \left(\frac{d\tilde{\dot{\epsilon}}}{d\tilde{z}}\right)\left(\frac{d^2\tilde{\dot{\epsilon}}}{d\tilde{z}^2}\right)N_2(\epsilon_1)(2\Delta\tilde{x}^2), \\ (\tilde{U}_s)_z = {} & 16\tilde{\dot{\epsilon}}_{max}^2(1 - 2\alpha - 2\tilde{z})\left(N_1(\epsilon_1)(\alpha + \tilde{z})(1 - \alpha - \tilde{z})\right. \\ & \left. - 4N_2(\epsilon_1)(\Delta\tilde{x}^2)\right). \end{aligned} \tag{12}$$

TABLE II. Relevant parameters for the second-order fluid model for particle migration in an extensional flow. In these expressions, $\tilde{x}$, $\tilde{x}_0$, $\tilde{y}$, $\tilde{y}_0$, and $\tilde{\dot{\epsilon}}$ are dimensionless and $\tilde{\dot{\epsilon}} = \tilde{\dot{\epsilon}}(\tilde{z})$.

β_{ij}	e_{ij}	γ_{ijk}	ψ_{ijk}
			$\psi_{111} = \frac{1}{5}\left(\frac{d^2\tilde{\dot{\epsilon}}}{d\tilde{z}^2}\right)(\tilde{x} - \tilde{x_0})$
			$\psi_{112} = \psi_{121} = \psi_{211} = \frac{-1}{15}\left(\frac{d^2\tilde{\dot{\epsilon}}}{d\tilde{z}^2}\right)(\tilde{y} - \tilde{y}_0)$
$\beta_{11} = -\tilde{\dot{\epsilon}}$	$e_{11} = -\tilde{\dot{\epsilon}}$	$\gamma_{113} = \gamma_{131} = \frac{-d\tilde{\dot{\epsilon}}}{d\tilde{z}}$	$\psi_{113} = \psi_{131} = \psi_{311} = \frac{-2}{3}\left(\frac{d\tilde{\dot{\epsilon}}}{d\tilde{z}}\right)$
$\beta_{22} = \tilde{\dot{\epsilon}}$	$e_{22} = \tilde{\dot{\epsilon}}$	$\gamma_{133} = \frac{-d^2\tilde{\dot{\epsilon}}}{d\tilde{z}^2}(\tilde{x} - \tilde{x}_0)$	$\psi_{122} = \psi_{212} = \psi_{221} = \frac{1}{15}\left(\frac{d^2\tilde{\dot{\epsilon}}}{d\tilde{z}^2}\right)(\tilde{x} - \tilde{x}_0)$
$\beta_{13} = \frac{-d\tilde{\dot{\epsilon}}}{d\tilde{z}}(\tilde{x} - \tilde{x}_0)$	$e_{13} = e_{31} = \frac{-1}{2}\left(\frac{d\tilde{\dot{\epsilon}}}{d\tilde{z}}\right)(\tilde{x} - \tilde{x}_0)$	$\gamma_{223} = \gamma_{232} = \frac{d\tilde{\dot{\epsilon}}}{d\tilde{z}}$	$\psi_{133} = \psi_{313} = \psi_{331} = \frac{-4}{15}\left(\frac{d^2\tilde{\dot{\epsilon}}}{d\tilde{z}^2}\right)(\tilde{x} - \tilde{x}_0)$
$\beta_{23} = \frac{d\tilde{\dot{\epsilon}}}{d\tilde{z}}(\tilde{y} - \tilde{y}_0)$	$e_{23} = e_{32} = \frac{1}{2}\left(\frac{d\tilde{\dot{\epsilon}}}{d\tilde{z}}\right)(\tilde{y} - \tilde{y}_0)$	$\gamma_{233} = \frac{d^2\tilde{\dot{\epsilon}}}{d\tilde{z}^2}(\tilde{y} - \tilde{y}_0)$	$\psi_{222} = \frac{-1}{5}\left(\frac{d^2\tilde{\dot{\epsilon}}}{d\tilde{z}^2}\right)(\tilde{y} - \tilde{y}_0)$
The rest = 0	The rest = 0	The rest = 0	$\psi_{223} = \psi_{232} = \psi_{322} = \frac{2}{3}\left(\frac{d\tilde{\dot{\epsilon}}}{d\tilde{z}}\right)$
			$\psi_{233} = \psi_{323} = \psi_{332} = \frac{4}{15}\left(\frac{d^2\tilde{\dot{\epsilon}}}{d\tilde{z}^2}\right)(\tilde{y} - \tilde{y}_0)$
			The rest = 0

θ_{ij}	τ_i	$e_{nm}\psi_{mni}$ $(i = 3)$
		$e_{11}\psi_{113} = e_{22}\psi_{223} = \frac{2}{3}\tilde{\dot{\epsilon}}\left(\frac{d\tilde{\dot{\epsilon}}}{d\tilde{z}}\right)$
$\theta_{12} = \theta_{21} = -2\left(\frac{d\tilde{\dot{\epsilon}}}{d\tilde{z}}\right)$		$e_{13}\psi_{313} = e_{31}\psi_{133} = \frac{2}{15}\left(\frac{d\tilde{\dot{\epsilon}}}{d\tilde{z}}\right)\left(\frac{d^2\tilde{\dot{\epsilon}}}{d\tilde{z}^2}\right)(\tilde{x} - \tilde{x}_0)^2$
$\theta_{31} = \left(\frac{-d^2\tilde{\dot{\epsilon}}}{d\tilde{z}^2}\right)(\tilde{y} - \tilde{y}_0)$	$\tau_1 = \left(\frac{-d^2\tilde{\dot{\epsilon}}}{d\tilde{z}^2}\right)(\tilde{x} - \tilde{x}_0)$	$e_{23}\psi_{323} = e_{32}\psi_{233} = \frac{2}{15}\left(\frac{d\tilde{\dot{\epsilon}}}{d\tilde{z}}\right)\left(\frac{d^2\tilde{\dot{\epsilon}}}{d\tilde{z}^2}\right)(\tilde{y} - \tilde{y}_0)^2$
$\theta_{32} = \left(\frac{d^2\tilde{\dot{\epsilon}}}{d\tilde{z}^2}\right)(\tilde{x} - \tilde{x}_0)$	$\tau_2 = \left(\frac{d^2\tilde{\dot{\epsilon}}}{d\tilde{z}^2}\right)(\tilde{y} - \tilde{y}_0)$	The rest = 0
The rest = 0	The rest = 0	$e_{nm}\psi_{mn3} = \frac{4}{3}\tilde{\dot{\epsilon}}\left(\frac{d\tilde{\dot{\epsilon}}}{d\tilde{z}}\right) + \frac{4}{15}\left(\frac{d\tilde{\dot{\epsilon}}}{d\tilde{z}}\right)\left(\frac{d^2\tilde{\dot{\epsilon}}}{d\tilde{z}^2}\right)((\tilde{x} - \tilde{x}_0)^2 + (\tilde{y} - \tilde{y}_0)^2)$

$\epsilon_{imn}e_{ml}\theta_{ln}$ $(i = 3)$	$e_{im}\tau_m (i = 3)$
$\epsilon_{3mn}e_{ml}\theta_{ln} = -e_{21}\theta_{11} + e_{11}\theta_{12} - e_{22}\theta_{21} + e_{12}\theta_{22} - e_{23}\theta_{31} + e_{13}\theta_{32}$	$e_{3m}\tau_m = e_{31}\tau_1 + e_{32}\tau_2 + e_{33}\tau_3$
$\epsilon_{3mn}e_{ml}\theta_{ln} = 4\tilde{\dot{\epsilon}}\left(\frac{d\tilde{\dot{\epsilon}}}{d\tilde{z}}\right) + \frac{1}{2}\left(\frac{d\tilde{\dot{\epsilon}}}{d\tilde{z}}\right)\left(\frac{d^2\tilde{\dot{\epsilon}}}{d\tilde{z}^2}\right)\left((\tilde{x} - \tilde{x}_0)^2 + (\tilde{y} - \tilde{y}_0)^2\right)$	$e_{3m}\tau_m = \frac{1}{2}\left(\frac{d\tilde{\dot{\epsilon}}}{d\tilde{z}}\right)\left(\frac{d^2\tilde{\dot{\epsilon}}}{d\tilde{z}^2}\right)\left((\tilde{x} - \tilde{x}_0)^2 + (\tilde{y} - \tilde{y}_0)^2\right)$

For a broad class of viscoelastic fluids, $-0.6 < \epsilon_1 < -0.5$,[12,13] suggestive of a large positive first normal stress difference and a small negative second normal stress difference in simple shear flow. Here, we assume that $\epsilon_1 = -0.56$, which is a reasonable value that assumes a small second normal stress difference,[12,13] which yields $N_1(\epsilon_1) = -1.61$ and $N_2(\epsilon_1) = -0.098$. For ease of expression and integration, we set $N_1(\epsilon_1) = A = -1.61$ and $4N_2(\epsilon_1)(\Delta\tilde{x}^2) = B = -0.098$, where A and B are numerical constants. Reorganization of Eq. (12) leads to

$$\frac{d\tilde{z}'}{d\tilde{t}} = 16\tilde{\epsilon}_{max}^2(1-2\tilde{z}')(A\tilde{z}'(1-\tilde{z}')-B), \tag{13}$$

where we express particle position in the fixed frame using the dimensionless coordinate $\tilde{z}' = z'/l$, which enables comparison to experimental particle migration data. Equation (13) can be integrated to determine particle trajectories,

$$\int_{\tilde{z}_0'}^{\tilde{z}'(t)} \frac{d\tilde{z}'}{((1-2\tilde{z}')(A\tilde{z}'(1-\tilde{z}')-B))} = 16\tilde{\epsilon}_{max}^2 \int_{\tilde{t}_0}^{\tilde{t}_f} d\tilde{t} \tag{14}$$

which upon integration leads to the particle trajectory equation,

$$\log\left(\frac{(A(\tilde{z}'(t)-1)\tilde{z}'(t)+B)}{(A(\tilde{z}_0'-1)\tilde{z}_0'+B)}\frac{(2\tilde{z}_0'-1)^2}{(2\tilde{z}'(t)-1)^2}\right)/(A-4B) = 16\tilde{\epsilon}_{max}^2(\tilde{t}_f-\tilde{t}_0), \tag{15}$$

where $\tilde{z}_0'$ is the dimensionless initial position of the particle in the z-direction (in the fixed frame) and $\tilde{z}'(t)$ is dimensionless position of the particle in the z-direction (in the fixed frame) at time t. In fitting Eq. (15) to our particle migration trajectories, we achieve a qualitative match to our experimental results: that is, the functional form clearly fits the data via a sigmoidal shape of the average particle position in the z-direction as a function of time. However, in order to make quantitative predictions and comparisons with existing rheological measurements, we need to obtain a dimensionalized expression of Eq. (15).

To determine characteristic scales, we follow the approach of Ho and Leal,[12] who used the reciprocal theorem to determine the lateral force on particles in second-order fluids in shear flow, which gives rise to a migration velocity. Following this approach, the physical scales for particle velocity are

$$(U_s)_z = l\left(\frac{d\tilde{z}'}{dt}\right) \sim \alpha_2\dot{\epsilon}\left(\frac{d\dot{\epsilon}}{d\tilde{z}'}\right)\frac{a^2}{6\eta_0 l}. \tag{16}$$

Using the dimensional expression for $\dot{\epsilon} = 4\dot{\epsilon}_{max}\tilde{z}'(1-\tilde{z}')$, we obtain

$$(U_s)_z = l\left(\frac{d\tilde{z}'}{dt}\right) \sim \frac{16\alpha_2\dot{\epsilon}_{max}^2 a^2}{6\eta_0 l}$$
$$\frac{d\tilde{z}'}{dt} \sim \frac{8\alpha_2\dot{\epsilon}_{max}^2 a^2}{3\eta_0 l^2}. \tag{17}$$

Equation (17) reveals a characteristic time scale $(8\alpha_2\dot{\epsilon}_{max}^2 a^2/3\eta_0 l^2)^{-1}$, where the physical parameters are particle diameter $a = 0.84$ μm, microdevice channel height $l = 80$ μm, zero-shear viscosity η_0, and maximum strain rate $\dot{\epsilon}_{max}$ from PTV measurements. Inserting the scaling relation from Eq. (17) into Eq. (13), we arrive at

$$\frac{d\tilde{z}'}{dt} = \left(\frac{8\alpha_2\dot{\epsilon}_{max}^2 a^2}{3\eta_0 l^2}\right)(1-2\tilde{z}')\,(A\tilde{z}'\,(1-\tilde{z}')-B)\,. \tag{18}$$

After integration, we obtain the final analytical expression for particle migration,

$$\log\left(\frac{(A(\tilde{z}'(t)-1)\tilde{z}'(t)+B)}{(A(\tilde{z}_0'-1)\tilde{z}_0'+B)}\frac{(2\tilde{z}_0'-1)^2}{(2\tilde{z}'(t)-1)^2}\right)/(A-4B) = \left(\frac{8\alpha_2\dot{\epsilon}_{max}^2 a^2}{3\eta_0 l^2}\right)(t-t_0) = Ct. \tag{19}$$

In determining particle trajectories, we set $t_0 = 0$, and the fitting coefficient C (units of 1/s) carries information regarding the normal stress coefficient $\alpha_2 = \psi_1 + \psi_2$ (units of Pa s^2). By comparing the analytical expression in Eq. (19) with experimental particle migration trajectories, we obtain the best-fit coefficient C and thereby determine the second-order fluid constant α_2, which allows for determination of the extensional viscosity η_E, as described in Sec. III B.

B. Extensional viscosity for a second-order fluid

The total stress T_{ij} for a second-order fluid is given by the retarded motion expansion,[64]

$$T_{ij} = -P\delta_{ij} + \eta_o A_{ij(1)} + \alpha_1 A_{ij(2)} + \alpha_2 A_{ik(1)}A_{kj(1)}, \tag{20}$$

where $A_{ij(1)}$ and $A_{ij(2)}$ are the Rivlin-Ericksen tensors,[64] P is the pressure, δ_{ij} is the second-order isotropic tensor, and α_1 and α_2 are the second-order fluid constants. In this expression, the rate-of-strain tensor is

$$A_{ij(1)} = \partial v_i/\partial x_j + \partial v_j/\partial x_i, \tag{21}$$

where v_i is the fluid velocity and $A_{ij(2)}$ is the covariant convected derivative of $A_{ij(1)}$ such that

$$A_{ij(2)} = \partial A_{ij(1)}/\partial t + v_k\partial A_{ij(1)}/\partial x_k + A_{ik(1)}\partial v_k/\partial x_j + \partial v_k/\partial x_i A_{kj(1)}. \tag{22}$$

Viscometric functions such as first ψ_1 and second normal stress coefficient ψ_2 can be directly related to the second-order fluid constants,

$$\alpha_1 = (T_{xx} - T_{yy})/2\dot{\gamma}^2 = -\psi_1/2 \tag{23}$$

and

$$\alpha_2 = (T_{xx} - T_{zz})/\dot{\gamma}^2 = \psi_1 + \psi_2. \tag{24}$$

General expressions for these quantities in extensional flow are given by

$$\underline{\underline{A}}_{(1)} = \begin{bmatrix} -\dot{\epsilon}(1+b) & 0 & 0 \\ 0 & 2\dot{\epsilon} & 0 \\ 0 & 0 & -\dot{\epsilon}(1-b) \end{bmatrix},$$
$$\underline{\underline{A}}_{(1)} \cdot \underline{\underline{A}}_{(1)} = \begin{bmatrix} \dot{\epsilon}^2(1+b)^2 & 0 & 0 \\ 0 & 4\dot{\epsilon}^2 & 0 \\ 0 & 0 & \dot{\epsilon}^2(1-b)^2 \end{bmatrix}, \tag{25}$$
$$\underline{\underline{A}}_{(2)} = \begin{bmatrix} \dot{\epsilon}^2(1+b)^2 & 0 & 0 \\ 0 & 4\dot{\epsilon}^2 & 0 \\ 0 & 0 & \dot{\epsilon}^2(1-b)^2 \end{bmatrix},$$

where b is a numerical constant specifying the nature of the extensional flow.

The expressions in Eq. (25) can be inserted into Eq. (20), considering our case of planar extensional flow ($b = 1$) to obtain

$$\underline{\underline{T}} = \begin{bmatrix} -P - 2\eta_0\dot{\epsilon} + 4\dot{\epsilon}^2(\alpha_1 + \alpha_2) & 0 & 0 \\ 0 & -P + 2\eta_0\dot{\epsilon} + 4\dot{\epsilon}^2(\alpha_1 + \alpha_2) & 0 \\ 0 & 0 & -P \end{bmatrix}. \tag{26}$$

The expression for extensional viscosity is as follows:

$$\begin{aligned} \eta_1 &= \frac{T_{xx} - T_{yy}}{\dot{\epsilon}} = -4\eta_0, \\ \eta_2 &= \frac{T_{yy} - T_{zz}}{\dot{\epsilon}} = 2\eta_0 + 4\dot{\epsilon}(\alpha_1 + \alpha_2), \\ \eta_3 &= \frac{T_{xx} - T_{zz}}{\dot{\epsilon}} = -2\eta_0 + 4\dot{\epsilon}(\alpha_1 + \alpha_2). \end{aligned} \tag{27}$$

The viscosity η_2 is the expression for extensional viscosity η_E. Here, $\alpha_1 = -\psi_1/2$ and $\alpha_2 = \psi_1 + \psi_2$, and setting $\epsilon_1 = \alpha_1/\alpha_2 = -0.5\psi_1/(\psi_1 + \psi_2)$, we obtain

$$\eta_E = \frac{T_{yy} - T_{zz}}{\dot{\epsilon}} = 2\eta_0 + 4\alpha_2\dot{\epsilon}(1 + \epsilon_1). \tag{28}$$

IV. RESULTS

A. Particle migration in extensional flow

Particle migration experiments were performed using four different solutions: a Newtonian liquid (60% w/w sucrose solution, $\eta_s = 60$ cP, where η_s is the solvent viscosity), 1 c^* λ-DNA solution, 2.5 c^* λ-DNA solution, and a 10 c^* aqueous PEO solution. Figure 6 shows average particle migration trajectories from microfluidic experiments across a wide range of experimental conditions. For the migration trajectories shown in Fig. 6, individual data points represent averages over several single particle trajectories ($N \approx 10$) for each experimental condition. Particle trajectories in Newtonian solutions show no evidence of z-direction migration, whereas particles immersed in polymer solutions near or above the overlap concentration c^* exhibit significant z-direction migration for all polymer solutions examined in this work.

In polymer solutions, particle migration is symmetric in the transverse direction, such that particles initially positioned near the channel center in the z-direction migrate either towards the upper or lower surface with equal probability. However, once the particles begin to migrate in one direction, they continue along this path without reversing the direction. In this way, it was observed that particles migrate in the z-direction towards the direction of minimal strain rate in the x-y plane, which is consistent with prior results in shear flow.[4,12] Interestingly, in our experiments, strain rate $\dot{\epsilon}$ is maximum at the channel center and minimum at the walls (Fig. 2), so particles migrate towards the top/bottom surfaces which is the apparent opposite direction compared to Poiseuille flow of viscoelastic fluids, where particles were observed to migrate toward the channel center. Moreover, these experimental results clearly show that the magnitude of the particle migration velocity is strongly dependent on *Wi*.

Particle migration trajectories from the analytical model in Eq. (19) are plotted as dashed lines in Fig. 6, together with experimental data. In general, good agreement is observed between experiments and analytical results for all three polymer solutions. In comparing the analytical model to experimental results, we treated the second order fluid constant α_2 on the right-hand side of Eq. (19) as a fitting parameter, thereby enabling estimation of the normal stress coefficients. Moreover, we assume that $\epsilon_1 = -0.56$, which is a reasonable

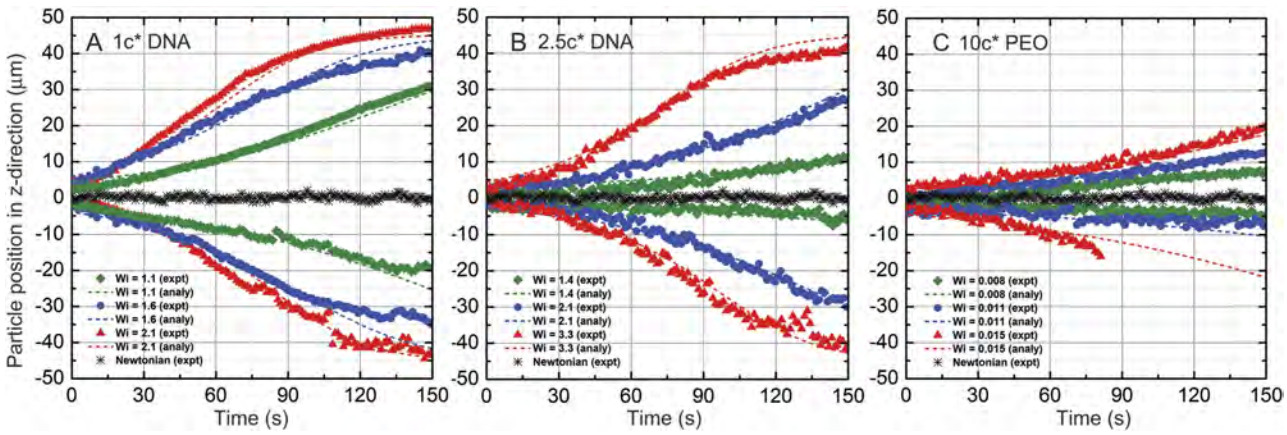

FIG. 6. Average particle migration trajectories in the transverse direction (z-direction) in planar extensional flow for (a) 1 c^* λ-DNA solution at $Wi = 1.1, 1.6, 2.1$, (b) 2.5 c^* λ-DNA solution at $Wi = 1.4, 2.1, 3.3$, and (c) 10 c^* PEO solution at $Wi = 0.008, 0.011, 0.015$. Experimental results are shown as data points for averages over multiple particle trajectory experiments ($N \approx 10$ for each case), and dashed lines show analytical results for particle trajectories from a second-order fluid model.

TABLE III. Polymer solution properties and extensional viscosities η_E measured using particle tracking and DoS rheometry.

Sample	η_E, microrheology (Pa s)	η_E, DoS rheometry (Pa s)
1 c^* DNA	$\eta_E = 93.6 \pm 3.6$, $Wi = 1.0$ $\eta_E = 88.2 \pm 4.6$, $Wi = 1.6$ $\eta_E = 96.9 \pm 4.6$, $Wi = 2.1$	η_E = 40–55, $Wi \geq 200$
2.5 c^* DNA	$\eta_E = 135.6 \pm 16.9$, $Wi = 1.4$ $\eta_E = 152.5 \pm 5.6$, $Wi = 2.1$ $\eta_E = 160.2 \pm 7.4$, $Wi = 3.3$	η_E = 100–180, $Wi \geq 200$
10 c^* PEO	$\eta_E = 45.6 \pm 2.8$, $Wi = 0.01$ $\eta_E = 39.4 \pm 2.1$, $Wi = 0.01$ $\eta_E = 31.0 \pm 2.2$, $Wi = 0.015$	η_E = 40–45, $Wi \geq 0.7$

value that assumes a small second normal stress difference. The zero-shear viscosity η_0 is independently measured in a series of steady-shear rheological experiments. Together, this approach allows for the estimation of the extensional viscosity η_E (Table III).

Particle migration trajectories were further plotted as a function of strain ϵ, as shown in Fig. 7. Here, the total strain experienced by fluid elements during migration events in the z-direction is obtained by integrating the z-dependent strain rate over the duration of the event,

$$\epsilon = \int_{t_i}^{t_f} \dot{\epsilon}\,(z(t))\,dt. \tag{29}$$

Using this approach, strain rates $\dot{\epsilon}(z(t))$ are experimentally determined using PTV, as shown in Fig. 2, followed by integration using Eq. (29) to determine strain. When plotted as a function of strain, particle migration trajectories are observed to collapse onto a single curve for different Wi for all three polymer solutions. These results suggest that the total strain experienced by individual particles governs the relative migration position in the microchannel, independent of Wi, in the regime of low to moderate flow rates or Wi.

B. DoS rheometry

Bulk extensional viscosity of polymer solutions was determined using the DoS (dripping-onto-substrate) rheometry protocols (Fig. 8),[44] which enables a direct comparison to η_E determined by microfluidic-based particle migration experiments. In DoS rheometry, transient and steady extensional viscosities η_E values are obtained as a function of the Hencky strain $\epsilon = 2\ln(R_o/R(t))$. The neck self-thinning dynamics are determined by the interplay of viscoelastic stresses $\dot{\epsilon}\eta_E$ contributed by polymer stretching and orientation and capillary stress σ/R that increases with a decrease in filament radius. All three polymer solutions show a significant amount of strain hardening (Fig. 8), and the strain-independent steady extensional viscosity values are at least two orders of magnitude larger than the zero-shear viscosity.

For both DNA and PEO solutions, transient extensional viscosity $\eta_E^{\dagger}(\dot{\epsilon}, \epsilon, t)$ values can also be measured from the intermediate thinning regime, with one important difference. Due to higher extensibility, the aqueous PEO solutions exhibit a pronounced elastocapillary response that is not observed for semi-dilute solutions of lower extensibility DNA chains. The observations for DNA solutions are in good agreement with the thinning behavior shown by low extensibility polysaccharides.[43] Furthermore, using DoS rheometry measurements of semi-dilute PEO solutions with five different molecular weights, Dinic *et al.* have shown that the extensional viscosity and extensional relaxation times for semi-dilute solutions are a strong function of extensibility.[46] The contrasting radius evolution profiles for DNA and PEO solutions are thus consistent with behavior expected based on chain extensibility.

The thinning dynamics in the elastocapillary regime (observed here only for PEO solutions) are typically described using the following approximate equation:[34,59]

$$\frac{R(t)}{R_o} \approx \left(\frac{G_E R_o}{2\sigma}\right)^{1/3} \exp\left(-t/3\lambda_E\right), \tag{30}$$

where R_o, G_E, and λ_E are the initial radius of the configuration, apparent elastic modulus, and the extensional relaxation time, respectively. When radius evolution over time is plotted on a semi-log plot (Fig. S4 of the supplementary material), the elastocapillary regime displays as a straight line, for the aqueous PEO solution with $c = 10\ c^*$, the extensional relaxation time $\lambda_E = 9.43 \pm 0.14$ ms was measured, and for $c = 1\ c^*$,

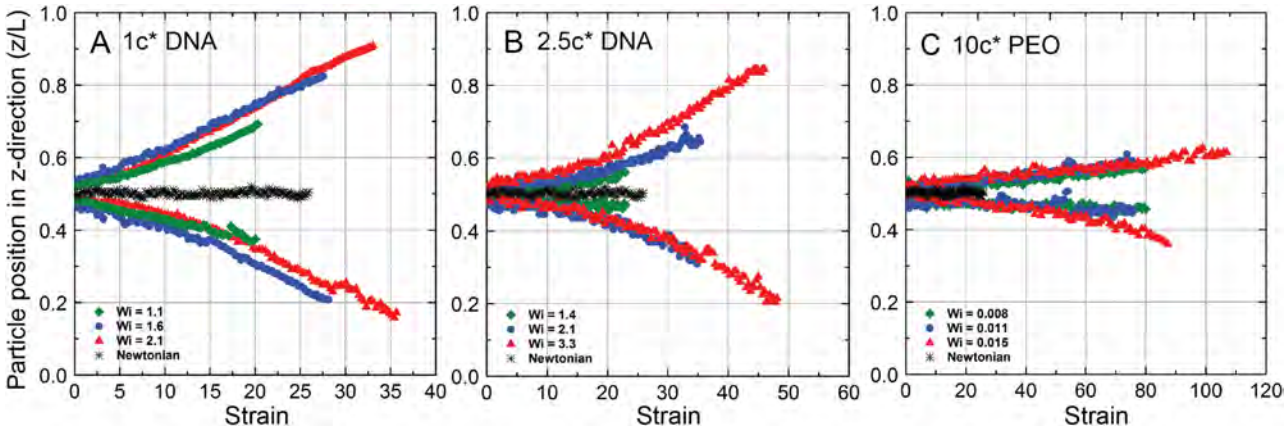

FIG. 7. Average particle migration trajectories in the transverse direction (z-direction) plotted as a function of total strain ϵ for (a) 1 c^* λ-DNA solution at Wi = 1.1, 1.6, 2.1, (b) 2.5 c^* λ-DNA solution at Wi = 1.4, 2.1, 3.3, and (c) 10 c^* PEO solution at Wi = 0.008, 0.011, 0.015. Particle position in the z-direction is non-dimensionalized with microchannel height l.

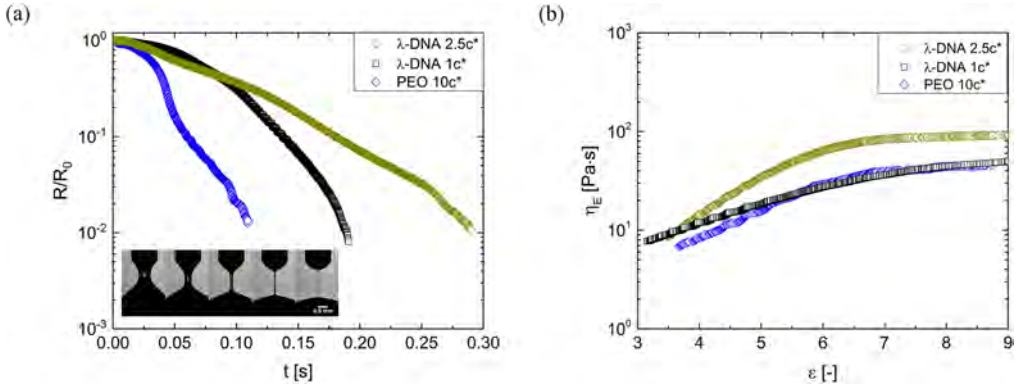

FIG. 8. Bulk measurement of extensional viscosity using the dripping-onto-substrate (DoS) technique. (a) Neck radius evolution in time data for semi-dilute polymer solutions. Also shown are images of liquid bridge (capillary) formation for 1 c^* λ-DNA solutions. (b) Transient and steady extensional viscosities as a function of the Hencky strain ϵ are computed using the radius evolution data for three solutions.

we found that $\lambda_E = 2.27 \pm 0.07$ ms. The measured value of the extensional relaxation time for the 10 c^* PEO solution is comparable to the relaxation time value obtained using linear viscoelastic response measured with oscillatory shear rheometry. During the elastocapillary phase of the thinning process, a homogeneous extensional flow with a constant and self-selected extension rate (dependent on the extensional relaxation time) is established within the neck. The transient extensional viscosity $\eta_E^+(\dot{\epsilon}, \epsilon, t)$ measured in the elastocapillary region shows significant concentration-dependent strain hardening, even though the steady shear viscosity measurements show a shear thinning response for semi-dilute PEO solutions.[46] Although the extension rate remains constant during elastocapillary thinning, the Hencky strain grows linearly in time. In the last regime before pinch-off, the extensional viscosity reaches a steady-state value. The extension rate and Hencky strain continue to increase, reaching extremely high values (see Table III and Figs. S4–S6 of the supplementary material). Quantitative measurements of the rheological response at such high extensional rates (or high *Wi*) are extremely challenging in microfluidic channels due to the influence of shear flows and onset of elastic instabilities.[47,48]

V. DISCUSSION

In general, extensional viscosity η_E values determined from particle migration microfluidic experiments are in reasonable agreement with values from DoS rheometry (Table III). These results indicate that the second-order fluid model is capable of accurately describing particle migration in viscoelastic fluids with mild departures from Newtonian behavior. Moreover, these results show that particle migration is driven by normal stress differences, which can be directly related to extensional viscosity. These arguments speak to the utility of using flow-based particle trapping methods via the Stokes trap to measure fundamental properties of complex fluids.

Extensional viscosities η_E determined from particle migration are steady-state extensional viscosities, corresponding to the plateau values of η_E obtained in DoS experiments. Despite the fact that microfluidic experiments and DoS rheometry were performed at different *Wi*, the extensional viscosities for polymer solutions measured in DoS were determined in the terminal regime (strain $\epsilon \approx 6$). Using the Stokes trap, we have the ability to effectively trap single particles for extremely long times (or strains) in extensional flow during a migration event. In the context of microfluidic experiments, polymer solutions are continuously flowing under steady-state conditions, and the total accumulated strain from the perspective of the suspended particles is very large ($\epsilon \geq 10$). Based on these arguments, we posit that microfluidic measurements of extensional viscosity can be directly compared to the terminal steady-state values of extensional viscosity from DoS measurements. Importantly, the terminal steady extensional viscosity is thought to represent a true material property[60,61] that depends on polymer concentration and/or molecular weight, but not on the extension rate or the accumulated strain.[61–63] Our results are consistent with this interpretation.

As a final comment on extensional viscosity values, we can estimate the steady extensional viscosity for relatively dilute polymer solutions using kinetic theory. In particular, the steady extensional viscosity can be estimated for a dilute polymer solution by solving the Smoluchowski equation for a polymer chain with finite extensibility using the preaveraging approximation, together with the Kramers expression for the steady-state stress.[66] Using this approach, the steady extensional viscosity for a dilute polymer solution can be estimated as $\eta_E = 2B\eta_{p,o}$, where $B = 3L^2/\langle R^2\rangle_o$, L is the polymer contour length, $\langle R^2\rangle_o$ is the equilibrium root-mean-square end-to-end distance, and $\eta_{p,o} = \eta_0 - \eta_s$ is the polymer contribution to the zero-shear viscosity.[66] These molecular-based expressions are highly amenable to analysis using single molecule experiments. In the case of unlabeled λ-phage DNA, $L = 16.3$ μm and $\langle R^2\rangle_o^{0.5} \approx 1.3$ μm,[67] determined using the relation $R_g = \langle R^2\rangle_o^{0.5}/\sqrt{6}$, where R_g is the polymer radius of gyration. For our microfluidic experiments at 1 c^* and 2.5 c^* DNA, the polymer contribution to the zero-shear viscosity is $\eta_{p,0} = 0.36$ Pa s^2 and 0.25 Pa s^2, respectively. Using these parameters, we estimate a steady extensional viscosity of $\eta_E \approx 60$ Pa s^2 and $\eta_E \approx 200$ Pa s^2 for 1 c^* and 2.5 c^* DNA solutions, respectively, which is in reasonable (order-of-magnitude) agreement with the extensional viscosity values in Table III. We emphasize that this expression for extensional viscosity

is only an estimate, lacking numerical prefactors. In addition, this expression is intended for relatively dilute polymer solutions, and it is expected to break down at higher polymer concentrations where the effects of intermolecular interactions in semi-dilute solutions begin to play a role in dynamics.[46,53,68]

From a broad perspective, this work extends microrheological techniques to a new realm of non-equilibrium measurements. Recent work in microrheology has focused on either passive methods based on particle diffusion or active methods that utilize an external force exerted on a particle (via an optical or magnetic trap) to perturb local microstructure away from equilibrium.[69,70] However, in our work, particles are freely suspended in a flowing flow, and hydrodynamic trapping (via a Stokes trap) allows for determination of non-equilibrium fluid properties without applying an external force to individual particles. In this way, this approach allows for microscale particle motion to be related to bulk-level materials response without using optical tweezers or external force fields. Overall, this work presents a new method for determining extensional viscosity using microfluidics that can be described as passive non-linear microrheology.

SUPPLEMENTARY MATERIAL

See supplementary material for the zero-shear viscosity and linear viscoelasticity measurements of polymer solutions (Figs. S1 and S2); particle migration trajectories and particle tracking data (Fig. S3); dripping-onto-substrate rheological data on polymer solutions (Figs. S4–S6).

ACKNOWLEDGMENTS

We thank Simon Rogers and Ching-Wei Lee for bulk rheology measurements and Anish Shenoy for assistance with particle trapping. We also thank Randy Ewoldt and Folarin Latinwo for insightful discussions. This work was funded by a Dow Graduate Fellowship for KWH and NSF CBET Award No. 1604038 and the David and Lucile Packard Foundation for CMS. V.S. thanks the UIC College of Engineering and the Department of Chemical Engineering for start-up funds and also acknowledges an initiation grant from the Campus Research Board (CRB) at UIC.

[1] D. Leighton and A. Acrivos, "The shear-induced migration of particles in concentrated suspensions," J. Fluid Mech. **181**, 415 (1987).
[2] J. R. Abbott, N. Tetlow, and A. L. Graham, "Experimental observations of particle migration in concentrated suspensions: Couette flow," J. Rheol. **35**, 773 (1991).
[3] A. Deboeuf, G. Gauthier, J. Martin, Y. Yurkovetsky, and J. F. Morris, "Particle pressure in a sheared suspension: A bridge from osmosis to granular dilatancy," Phys. Rev. Lett. **102**, 108301 (2009).
[4] A. Karnis and S. G. Mason, "Particle motions in sheared suspensions. XIX. Viscoelastic media," Trans. Soc. Rheol. **10**, 571 (1966).
[5] A. B. Metzner, Y. Cohen, and C. Rangel-Nafaile, "Inhomogeneous flows of non-Newtonian fluids: Generation of spatial concentration gradients," J. Non-Newtonian Fluid Mech. **5**, 449 (1979).
[6] U. S. Agarwal, A. Dutta, and R. A. Mashelkar, "Migration of macromolecules under flow: The physical origin and engineering implications," Chem. Eng. Sci. **49**, 1693 (1994).
[7] H. Zhao and E. S. G. Shaqfeh, "Shear-induced platelet margination in a microchannel," Phys. Rev. E **83**, 061924 (2011).
[8] R. G. Henríquez Rivera, K. Sinha, and M. D. Graham, "Margination regimes and drainage transition in confined multicomponent suspensions," Phys. Rev. Lett. **114**, 188101 (2015).
[9] R. Fahraeus and T. Lindqvist, "The viscosity of the blood in narrow capillary tubes," Am. J. Physiol. **96**, 562 (1931).
[10] H. Ma and M. D. Graham, "Theory of shear-induced migration in dilute polymer solutions near solid boundaries," Phys. Fluids **17**, 083103 (2005).
[11] B. P. Ho and L. G. Leal, "Inertial migration of rigid spheres in two-dimensional unidirectional flows," J. Fluid Mech. **65**, 365 (1974).
[12] B. P. Ho and L. G. Leal, "Migration of rigid spheres in a two-dimensional unidirectional shear flow of a second-order fluid," J. Fluid Mech. **76**, 783 (1976).
[13] P. C.-H. Chan and L. G. Leal, "A note on the motion of a spherical particle in a general quadratic flow of a second-order fluid," J. Fluid Mech. **82**, 549 (1977).
[14] P. R. Nott and J. F. Brady, "Pressure-driven suspension flow: Simulation and theory," J. Fluid Mech. **275**, 157 (1994).
[15] J. F. Morris and F. Boulay, "Curvilinear flows of noncolloidal suspensions: The role of normal stresses," J. Rheol. **43**, 1213 (1999).
[16] M. Frank, D. Anderson, E. R. Weeks, and J. F. Morris, "Particle migration in pressure-driven flow of a Brownian suspension," J. Fluid Mech. **493**, 363 (2003).
[17] J. F. Morris, "A review of microstructure in concentrated suspensions and its implications for rheology and bulk flow," Rheol. Acta **48**, 909 (2009).
[18] S. Garland, G. Gauthier, J. Martin, and J. F. Morris, "Normal stress measurements in sheared non-Brownian suspensions," J. Rheol. **57**, 71 (2013).
[19] X. Lu, C. Liu, X. Hu, and G. Xuan, "Particle manipulations in non-Newtonian microfluidics: A review," J. Colloid Interface Sci. **500**, 182–201 (2017).
[20] F. Del Guidice, G. D'Avino, F. Greco, I. De Santo, P. A. Netti, and P. L. Maffettone, "Rheometry-on-a-chip: Measuring the relaxation time of a viscoelastic liquid through particle migration in microchannel flows," Lab Chip **15**, 783–792 (2015).
[21] E. J. Lim, T. J. Ober, J. F. Edd, S. P. Desai, D. Neal, K. W. Bong, P. S. Doyle, G. H. McKinley, and M. Toner, "Inertio-elastic focusing of bioparticles in microchannels at high throughput," Nat. Commun. **5**, 4120 (2014).
[22] G. G. Fuller and L. G. Leal, "Flow birefringence of concentrated polymer solutions in two-dimensional flows," J. Polym. Sci., Polym. Phys. Ed. **19**, 557 (1981).
[23] R. C.-Y. Ng and L. G. Leal, "Concentration effects on birefringence and flow modification of semidilute polymer solutions in extensional flows," J. Rheol. **37**, 443 (1993).
[24] A. Keller and J. A. Odell, "The extensibility of macromolecules in solution: A new focus for macromolecular science," Colloid Polym. Sci. **263**, 181–201 (1985).
[25] J. A. Odell and S. P. Carrington, "Extensional flow oscillatory rheometry," J. Non-Newtonian Fluid Mech. **137**, 110–120 (2006).
[26] S. J. Haward, V. Sharma, and J. A. Odell, "Extensional opto-rheometry with biofluids and ultra-dilute polymer solutions," Soft Matter **7**, 9908–9921 (2011).
[27] S. J. Haward, M. S. N. Oliveria, M. A. Alves, and G. H. McKinley, "Optimized cross-slot flow geometry for microfluidic extensional rheometry," Phys. Rev. Lett. **109**, 128301 (2012).
[28] S. J. Haward, "Microfluidic extensional rheometry using stagnation point flow," Biomicrofluidics **10**, 043401 (2016).
[29] V. Tirtaatmadja and T. Sridhar, "Filament-stretching device for measurement of extensional viscosity," J. Rheol. **37**, 1081–1102 (1993).
[30] R. K. Gupta, D. A. Nguyen, and T. Sridhar, "Extensional viscosity of dilute polystyrene solutions: Effect of concentration and molecular weight," Phys. Fluids **12**, 1296–1318 (2000).
[31] G. H. McKinley and T. Sridhar, "Filament-stretching rheometry of complex fluids," Annu. Rev. Fluid. Mech. **34**, 375 (2002).
[32] S. L. Anna and G. H. McKinley, "Elasto-capillary thinning and breakup of model elastic liquids," J. Rheol. **45**, 115–138 (2001).
[33] L. E. Rodd, T. P. Scott, J. J. Cooper-White, and G. H. McKinley, "Capillary breakup rheometry of low-viscosity elastic fluids," Appl. Rheol. **15**, 12 (2005).
[34] G. H. McKinley, "Visco-elasto-capillary thinning and break-up of complex fluids," Rheol. Rev. **1**, 1 (2005).
[35] S. J. Haward, V. Sharma, C. P. Butts, G. H. McKinley, and S. S. Rahatekar, "Shear and extensional rheology of cellulose/ionic liquid solutions," Biomacromolecules **13**, 1688–1699 (2012).

[36]O. Arnolds, H. Buggisch, D. Sachsenheimer, and N. Willenbacher, "Capillary breakup extensional rheometry (caber) on semi-dilute and concentrated polyethyleneoxide solutions," Rheol. Acta **49**, 1207–1217 (2010).
[37]L. Campo-Deano and C. A. Clasen, "The slow retraction method (SRM) for the determination of ultra-short relaxation times in capillary breakup extensional rheometry experiments," J. Non-Newtonian Fluid Mech. **165**, 1688–1699 (2010).
[38]P. E. Arratia, J. P. Gollub, and D. J. Durian, "Polymeric filament thinning and breakup in microchannels," Phys. Rev. E **77**, 036309 (2008).
[39]P. E. Arratia, L. Cramer, J. P. Gollub, and D. J. Durian, "The effects of polymer molecular weight on filament thinning and drop breakup in microchannels," New J. Phys. **11**, 115006 (2009).
[40]F. Ingremeau and H. Kellay, "Stretching polymers in droplet-pinch-off experiments," Phys. Rev. X **3**, 041002 (2013).
[41]S. Sachdev, A. Muralidharan, and P. E. Boukany, "Molecular processes leading to necking in extensional flow," Macromolecules **49**, 9578–9585 (2016).
[42]A. Ardekani, V. Sharma, and G. H. McKinley, "Dynamics of bead formation, filament thinning and breakup of weakly viscoelastic jets," J. Fluid Mech. **665**, 46–56 (2010).
[43]V. Sharma, S. J. Haward, J. Serdy, B. Keshavarz, A. Soderlund, P. Threlfall-Holmes, and G. H. McKinley, "The rheology of aqueous solutions of ethyl hydroxy-ethyl cellulose (EHEC) and its hydrophobically modified analogue (hmEHEC): Extensional flow response in capillary break-up, jetting (ROJER) and in a cross-slot extensional rheometer," Soft Matter **11**, 3251 (2015).
[44]J. Dinic, Y. Zhang, L. N. Jimenez, and V. Sharma, "Extensional relaxation times of dilute, aqueous polymer solutions," ACS Macro Lett. **4**, 804 (2015).
[45]J. Dinic, L. N. Jimenez, and V. Sharma, "Pinch-off dynamics and dripping-onto-substrate (DoS) rheometry of complex fluids," Lab Chip **17**, 460 (2017).
[46]J. Dinic, M. Biagioli, and V. Sharma, "Pinch-off dynamics and extensional relaxation times of intrinsically semi-dilute polymer solutions characterized by dripping-onto-substrate rheometry," J. Polym. Sci. B: Polym. Phys. (published online 2017).
[47]T. J. Ober, S. J. Haward, C. J. Pipe, J. Soulages, and G. H. McKinley, "Microfluidic extensional rheometry using a hyperbolic contraction geometry," Rheol. Acta **52**, 529 (2013).
[48]D. F. James, "N_1 stresses in extensional flows," J. Non-Newtonian Fluid Mech. **232**, 33–42 (2016).
[49]F. J. Galindo-Rosales, M. A. Alves, and M. S. N. Oliveria, "Microdevices for extensional rheometry of low viscosity elastic liquids: A review," Microfluid. Nanofluid. **14**, 1–19 (2013).
[50]M. Tanyeri, M. Ranka, N. Sittipolkul, and C. M. Schroeder, "A microfluidic-based hydrodynamic trap: Design and implementation," Lab Chip **11**, 1786 (2011).
[51]A. Shenoy, C. V. Rao, and C. M. Schroeder, "Stokes trap for multiplexed particle manipulation and assembly using fluidics," Proc. Natl. Acad. Sci. U. S. A. **113**, 3976 (2016).
[52]S. Pan, D. At Nguyen, T. Sridhar, P. Sunthar, and R. J. Prakash, "Universal solvent quality crossover of the zero shear rate viscosity of semidilute DNA solutions," J. Rheol. **58**, 339 (2014).
[53]K. Hsiao, C. Sasmal, J. R. Prakash, and C. M. Schroeder, "Direct observation of DNA dynamics in semidilute solutions in extensional flow," J. Rheol. **61**, 151 (2017).
[54]P. E. Arratia, C. C. Thomas, J. Diorio, and J. P. Gollub, "Elastic instabilities of polymer solutions in cross-channel flow," Phys. Rev. Lett. **96**, 144502 (2006).
[55]P. P. Bhat, S. Appathurai, M. T. Harris, and O. A. Basaran, "On self-similarity in the drop-filament corner region formed during pinch-off of viscoelastic fluid threads," Phys. Fluids **24**, 083101 (2012).
[56]R. Suryo and O. A. Basaran, "Local dynamics during pinch-off of liquid threads of power law fluids: Scaling analysis and self-similarity," J. Non-Newtonian Fluid Mech. **138**, 134 (2006).
[57]D. T. Papageorgiou, "On the breakup of viscous liquid threads," Phys. Fluids **7**, 1529 (1995).
[58]G. H. McKinley and A. Tripathi, "How to extract the Newtonian viscosity from capillary breakup measurements in a filament rheometer," J. Rheol. **44**, 653 (2000).
[59]V. Entov and E. J. Hinch, "Effect of a spectrum of relaxation times on the capillary thinning of a filament of elastic liquid," J. Non-Newtonian Fluid Mech. **72**, 31 (1997).
[60]M. Stelter, G. Brenn, A. L. Yarin, R. P. Singh, and F. Durst, "Validation and application of a novel elongational device for polymer solutions," J. Rheol. **44**, 595 (2000).
[61]M. Stelter, G. Brenn, A. L. Yarin, R. P. Singh, and F. Durst, "Investigation of the elongational behavior of polymer solutions by means of an elongational rheometer," J. Rheol. **46**, 507 (2002).
[62]V. M. Entov and A. L. Yarin, "Influence of elastic stresses on the capillary breakup of jets of dilute polymer solutions," Fluid Dyn. **19**, 21 (1984).
[63]D. F. James and T. Sridhar, "Molecular conformation during steady-state measurements of extensional viscosity," J. Rheol. **39**, 713 (1995).
[64]R. Bird, R. Armstrong, and O. Hassager, *Dynamics of Polymeric Liquids* (Wiley, New York, NY, 1987), Vol. 1.
[65]M. Tanyeri and C. M. Schroeder, "Manipulation and confinement of single particles using fluid flow," Nano Lett. **13**, 2357 (2013).
[66]R. G. Larson, *The Structure and Rheology of Complex Fluids* (Oxford University Press, 1999).
[67]D. E. Smith, T. T. Perkins, and S. Chu, "Dynamical scaling of DNA diffusion coefficients," Macromolecules **29**, 1372–1373 (1996).
[68]R. Prabhaker, S. Gadkari, T. Gopesh, and M. J. Shaw, "Influence of stretching induced self-concentration and self-dilution on coil-stretch hysteresis and capillary thinning of unentangled polymer solutions," J. Rheol. **60**, 345–366 (2016).
[69]R. N. Zia and J. F. Brady, "Microviscosity, microdiffusivity, and normal stresses in colloidal dispersions," J. Rheol. **56**, 1175 (2012).
[70]C. D. Chapman and R. M. Robertson-Anderson, "Nonlinear microrheology reveals entanglement-driven molecular-level viscoelasticity of concentrated DNA," Phys. Rev. Lett. **113**, 098303 (2014).